Aberration compensation in aplanatic solid immersion lens microscopy

Yang Lu,[1] Thomas Bifano,[2] Selim Ünlü,[2] and Bennett Goldberg[2,*]

[1]*Department of Mechanical Engineering, Boston University, 110 Cummington Mall, Boston, MA, 02215, USA*
[2]*Boston University Photonics Center, 8 Saint Mary's Street, Boston, MA, 02215, USA*
**goldberg@bu.edu*

Abstract: The imaging quality of an aplanatic SIL microscope is shown to be significantly degraded by aberrations, especially when the samples have thicknesses that are more than a few micrometers thicker or thinner than the design thickness. Aberration due to the sample thickness error is modeled and compared with measurements obtained in a high numerical aperture (NA ~3.5) microscope. A technique to recover near-ideal imaging quality by compensating aberrations using a MEMS deformable mirror is described and demonstrated.

OCIS codes: (110.1085) Adaptive imaging; (220.1000) Aberration compensation.

References and links

1. S. M. Mansfield and G. S. Kino, "Solid Immersion Microscope," Appl. Phys. Lett. **57**(24), 2615–2616 (1990).
2. L. P. Ghislain and V. B. Elings, "Near-field scanning solid immersion microscope," Appl. Phys. Lett. **72**(22), 2779–2781 (1998).
3. D. A. Fletcher, K. B. Crozier, C. F. Quate, G. S. Kino, K. E. Goodson, D. Simanovskii, and D. V. Palanker, "Near-field infrared imaging with a microfabricated solid immersion lens," Appl. Phys. Lett. **77**(14), 2109–2111 (2000).
4. K. Karrai, X. Lorenz, and L. Novotny, "Enhanced reflectivity contrast in confocal solid immersion lens microscopy," Appl. Phys. Lett. **77**(21), 3459–3461 (2000).
5. J. Zhang, C. W. See, and M. G. Somekh, "Imaging performance of widefield solid immersion lens microscopy," Appl. Opt. **46**(20), 4202–4208 (2007).
6. S. B. Ippolito, B. B. Goldberg, and M. S. Ünlü, "High spatial resolution subsurface microscopy," Appl. Phys. Lett. **78**(26), 4071–4073 (2001).
7. E. Ramsay, K. A. Serrels, M. J. Thomson, A. J. Waddie, M. R. Taghizadeh, R. J. Warburton, and D. T. Reid, "Three-dimensional nanoscale subsurface optical imaging of silicon circuits," Appl. Phys. Lett. **90**(13), 131101 (2007).
8. E. Ramsay, N. Pleynet, D. Xiao, R. J. Warburton, and D. T. Reid, "Two-photon optical-beam-induced current solid-immersion imaging of a silicon flip chip with a resolution of 325 nm," Opt. Lett. **30**(1), 26–28 (2005).
9. S. B. Ippolito, B. B. Goldberg, and M. S. Ünlü, "Theoretical analysis of numerical aperture increasing lens microscopy," J. Appl. Phys. **97**(5), 053105 (2005).
10. F. H. Köklü, J. I. Quesnel, A. N. Vamivakas, S. B. Ippolito, B. B. Goldberg, and M. S. Unlü, "Widefield subsurface microscopy of integrated circuits," Opt. Express **16**(13), 9501–9506 (2008).
11. F. H. Köklü and M. S. Unlü, "Subsurface microscopy of interconnect layers of an integrated circuit," Opt. Lett. **35**(2), 184–186 (2010).
12. P. Török, "Focusing of electromagnetic waves through a dielectric interface by lenses of finite Fresnel number," J. Opt. Soc. Am. A **15**(12), 3009–3015 (1998).
13. M. Lang, E. Aspnes, and T. D. Milster, "Geometrical analysis of third-order aberrations for a solid immersion lens," Opt. Express **16**(24), 20008–20028 (2008).
14. S. H. Goh and C. J. R. Sheppard, "High aperture focusing through a spherical interface: Application to refractive solid immersion lens (RSIL) for subsurface imaging," Opt. Commun. **282**(5), 1036–1041 (2009).
15. S. H. Goh, C. J. R. Sheppard, A. C. T. Quah, C. M. Chua, L. S. Koh, and J. C. H. Phang, "Design considerations for refractive solid immersion lens: Application to subsurface integrated circuit fault localization using laser induced techniques," Rev. Sci. Instrum. **80**(1), 013703 (2009).
16. R. Chen, K. Agarwal, C. J. R. Sheppard, J. C. H. Phang, and X. D. Chen, "Resolution of aplanatic solid immersion lens based microscopy," J. Opt. Soc. Am. A **29**(6), 1059–1070 (2012).
17. R. Chen, K. Agarwal, Y. Zhong, C. J. R. Sheppard, J. C. H. Phang, and X. D. Chen, "Complete modeling of subsurface microscopy system based on aplanatic solid immersion lens," J. Opt. Soc. Am. A **29**(11), 2350–2359 (2012).

#197853 - $15.00 USD Received 1 Oct 2013; revised 31 Oct 2013; accepted 31 Oct 2013; published 8 Nov 2013

18. R. Chen, K. Agarwal, C. J. R. Sheppard, J. C. H. Phang, and X. D. Chen, "A complete and computationally efficient numerical model of aplanatic solid immersion lens scanning microscope," Opt. Express **21**(12), 14316–14330 (2013).
19. T. X. Hoang, X. D. Chen, and C. J. R. Sheppard, "Rigorous analytical modeling of high-aperture focusing through a spherical interface," J. Opt. Soc. Am. A **30**(7), 1426–1440 (2013).
20. P. Kner, J. W. Sedat, D. A. Agard, and Z. Kam, "High-resolution wide-field microscopy with adaptive optics for spherical aberration correction and motionless focusing," J. Microsc. **237**(2), 136–147 (2010).
21. M. Schwertner, M. Booth, T. Tanaka, T. Wilson, and S. Kawata, "Spherical aberration correction system using an adaptive optics deformable mirror," Opt. Commun. **263**(2), 147–151 (2006).
22. M. Shaw, S. Hall, S. Knox, R. Stevens, and C. Paterson, "Characterization of deformable mirrors for spherical aberration correction in optical sectioning microscopy," Opt. Express **18**(7), 6900–6913 (2010).
23. E. J. Botcherby, R. Juskaitis, M. J. Booth, and T. Wilson, "Aberration-free optical refocusing in high numerical aperture microscopy," Opt. Lett. **32**(14), 2007–2009 (2007).
24. M. J. Booth, "Adaptive optics in microscopy," Philos Trans A Math Phys Eng Sci **365**(1861), 2829–2843 (2007).
25. Y. Lu, E. Ramsay, C. R. Stockbridge, A. Yurt, F. H. Köklü, T. G. Bifano, M. S. Ünlü, and B. B. Goldberg, "Spherical aberration correction in aplanatic solid immersion lens imaging using a MEMS deformable mirror," Microelectron. Reliab. **52**(9-10), 2120–2122 (2012).
26. R. R. Shannon and J. C. Wyant, "Basic Wavefront Aberration Theory for Optical Metrology," in *Applied Optics and Optical Engineering, Vol. 11* (Academic, 1992), Chap. 1.
27. M. J. Booth, M. A. A. Neil, and T. Wilson, "Aberration correction for confocal imaging in refractive-index-mismatched media," J. Microsc. **192**(2), 90–98 (1998).
28. M. J. Booth, D. Débarre, and A. Jesacher, "Adaptive optics for biomedical microscopy," Opt. Photonics News **23**(1), 22–29 (2012).

1. Introduction

Solid immersion lens (SIL) microscopy is a technique developed for high-resolution imaging through layers of high-index-of-refraction materials [1–4]. The technique employs a high-index-of-refraction hemispherical lens in direct contact with the substrate medium to enable high numerical aperture (NA) imaging [5–7]. One example application is solid immersion lens microscopy for semiconductor backside inspection [8–11]. By taking advantage of the high refractive index of silicon (Si) or gallium arsenide (GaAs) using near-infrared (NIR) illumination, the effective NA of the microscope can be significantly increased, thus higher resolution and better light collection efficiency can be achieved.

There are two major types of SILs, central SILs (cSILs) and aplanatic SILs (aSILs), both of which provide aberration free imaging at a single point. The convex surface of the SIL, which has spherical geometry, faces the backing objective of the microscope. The planar surface of the SIL is in contact with the substrate of the device under test (DUT). A cSIL focuses light to the center of the sphere defined by the convex surface when light incident arrive normal to that surface. In an aSIL, the incident light is not normal to the convex surface, and is refracted toward the focal point. An aSIL focuses light at the aplanatic point of the sphere, which is located at a distance R/n below the center of the super-hemisphere lens, as shown in Fig. 1, where R is the sphere radius and n the refractive index of the material [9]. For cSILs, the NA is limited by the maximum NA of the backing objective, whereas aSILs can reach the theoretical maximum NA of the medium index (3.5 for Si at 1310nm) even when using a relatively low NA backing objective (10 × - 20 ×). It is currently the only method that can achieve sufficient resolution to image the next generation of integrated circuits [10].

Recently, the theoretical behavior of the aSIL has been studied by several groups [5, 9, 12–19]. It was shown that aberration-free imaging is possible only at the aplanatic point of the sphere. Zhang *et al.* [5], Ippolito *et al.* [9] and Lang *et al.* [13] included aberration analysis using ray tracing in their aSIL modeling, and demonstrated that aSILs are highly susceptible to spherical aberration when the object to be imaged is located away from aplanatic point. Goh and Sheppard [14] later confirmed this aberration susceptibility to aSILs through wave analysis. In practical scenarios, the geometric tolerances used for thinning substrates make it challenging to ensure that the object to be imaged is located in the aplanatic plane (the axial plane containing the aplanatic point) with a precision better than +/–10 μm. A thickness-mismatched sample mainly introduces spherical aberration that lowers the peak intensity and adds side-lobes to the focal spot, consequently reducing the measured signal intensity. Although some groups have proposed open-loop spherical aberration control in different imaging modalities [20–22], most of them are in low NA domain (compared to a NA of 3.5 in solid immersion imaging). Because of the high NA nature of the aplanatic solid immersion lens microscopy, small sample thickness errors result in significant aberration, which greatly degrades imaging quality [23, 24]. In a previous study, we demonstrated the effect of such aberrations on the aSIL microscope point spread function. We proposed and successfully demonstrated that a MEMS deformable mirror (DM) can be used to counteract the spherical aberrations associated with non-ideal sample thickness [25].

Here we extend the aSIL aberration correction study to include a real test resolution structure, simulations on spherical aberration in a wider thickness mismatch range and a confocal scanning aSIL imaging system with multiple wavelengths and SIL materials. Below, we first model the spherical aberration versus sample thickness mismatch both using analytical model and ray tracing software (Zemax) to understand how much aberrations are in the system and how much can be compensated by the DM. Subsequently, we calibrate the DM shapes to nanometer precision to compensate the spherical aberration introduced by sample thickness error. Finally, we demonstrate that the DM can recover the system's theoretical resolving power in a confocal scanning aSIL microscope.

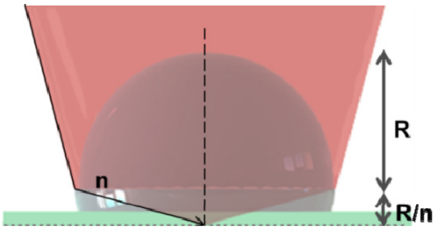

Fig. 1. Cross section of aplanatic SIL focusing geometry, drawn to scale. Illumination converging on the aSIL from a backing objective (not shown) is refracted toward the aplanatic point. The planar bottom surface of the aSIL contacts the planar upper surface of the sample, Focus is achieved at a depth *R/n* below the center of the sphere defined by the aSILs upper surface.

2. Simulation

The aSIL analytical model is based on Lang *et al.* method using geometrical analysis to find spherical aberration at different focal depth [13]. The key parameters for the modeling are shown in Fig. 1. Not shown in this figure is the backing objective, with a NA of 0.285. The aSIL has a radius of curvature (R) of 2.350 mm. Both the sample and the aSIL are made of Si. We assume that the index of refraction (n) for Si is 3.5 and that the illumination wavelength is 1310 nm. The aberration-free imaging plane is located at a depth of 671 μm (R/n) below the geometric center of the curved surface of the aSIL. The aSIL height is 2.922 mm, which matches with a designed sample thickness of 100 μm. In the model, we assume there is no air gap between SIL and sample. In the ray tracing software, we adjusted the distance between the paraxial lens and aSIL to produce minimum wavefront error in the imaging plane. We fit the modeled wavefront aberration error to a 37-term Zernike polynomial expansion neglecting the first three terms (piston, tip and tilt), which do not affect resolution.

In both cases, we varied the sample thickness with respect to the ideal sample thickness parametrically from −100 μm to + 10 μm (e.g. sample thicknesses from 0 μm to 110 μm) at 5 μm intervals and plotted the first order spherical term root mean square (RMS) amplitude as a function of substrate thickness error in Fig. 2. The analytical and ray tracing data exhibit good agreement on the trend of spherical aberration when sample thickness deviates from ideal thickness. However, the analytical model underestimates the amount of spherical aberration due to paraxial approximation in the calculation, as noted by Lang *et al* [13].

Figure 2 confirms the dominant aberration term is first order spherical aberration (Zernike term 11). Aberrations are much greater for thicker-than-ideal samples than for thinner-than-ideal samples. The amplitude of aberration reaches a maximum and then drops towards the central point (the other aberration free imaging point) for negative thickness errors (sample too thin), but increases sharply and without apparent bound for positive thickness errors (sample too thick). We also considered the off-axis aberration, which is from beam scanning, through ray trace. The scanning angle provides a field of view of ± 15μm. The results shows first order spherical wavefront error remains the largest component of the aberration.

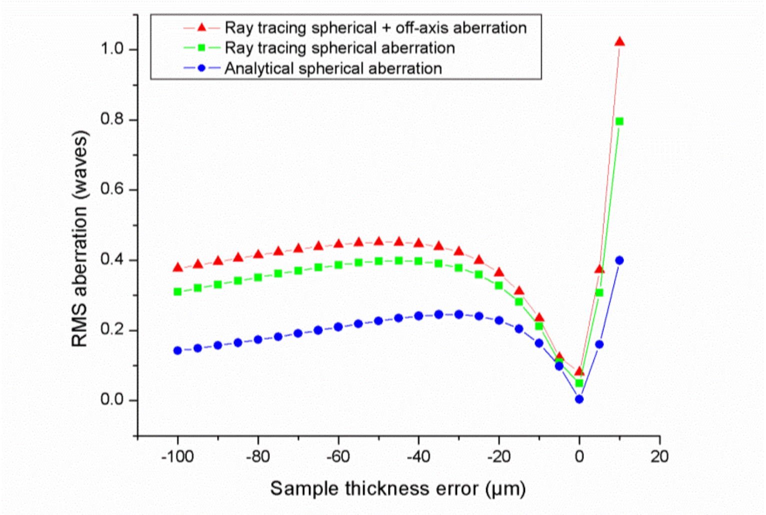

Fig. 2. Simulation of system aberration as a function of sample thickness error (deviation from design thickness) using analytical and ray tracing data. The results indicate that negative values of sample thickness error produce relatively smaller and more manageable aberrations than positive values of thickness error.

3. Experimental apparatus

3.1 DM shape calibration

After modeling aberrations in the aSIL, we calibrated the DM so that we could produce first order spherical shapes that would compensate sample-thickness-error-induced aberrations. In this study, a gold-coated continuous face-sheet MEMS DM (Boston Micromachines Corporation, Multi-DM) was used, see Fig. 3. It is comprised of a continuous membrane mirror supported by an underlying array of 140 actuators arranged on a 12 × 12 grid where the 4 corner actuators are inactive. Actuator pitch is 450 µm. Each actuator can impose a local surface-normal deflection on the mirror of up to 5 µm, with resolution of less than 1 nm. The DM pupil is conjugate to the microscope objective, and its active pupil area corresponds to a circular region measuring 4.05 mm. Consequently, about half of the actuators are within the aperture for which shape is to be controlled, and the remaining actuators are outside of that aperture. Since actuators outside of the shape-controlled aperture can affect mirror deformation inside of the aperture through mechanical coupling, all actuators are controlled actively in the calibration effort.

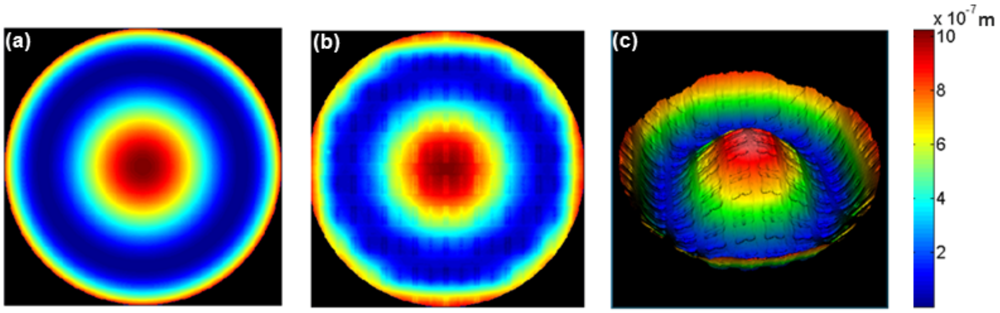

Fig. 3. Deformable mirror surface topography corresponding to a + 300 nm RMS first order spherical shape. (a): Math model of the desired shape. (b): Measurement of DM shape after closed-loop calibration. There is about 50 nm RMS residual error in the measured shape as compared to the desired shape. (c): Perspective view of the measured DM surface.

While any amount of aberration compensation will improve image quality, a well-corrected imaging system requires wavefront error RMS below λ/14 [26], which is 93 nm in this case (and 76 nm for 1064 nm wavelength illumination). Since shape errors on the DM are doubled by reflection in the wavefront, the DM shape errors should be made less than ~47 nm to achieve well-corrected imaging. The DM was calibrated using a surface mapping interferometer (ZYGO NewView 6300) in a closed-loop fashion with a goal of determining what input voltages to the 140 active actuators would produce a particular amplitude of first order spherical aberration within a 4.05 mm aperture with the least residual shape error. Residual shape errors (e.g. the difference between the current DM shape and the desired DM shape) were used in a closed-loop iterative feedback controller to make the DM shape converge to the desired shape, and then the corresponding array of input voltages to the DM actuators was stored for subsequent open-loop control experiments. We used this technique to determine first order spherical shapes with RMS amplitude from −500 nm to + 500 nm with 100 nm intervals, and then interpolate the data set for finer steps to estimate DM inputs to achieve arbitrary first order spherical aberration shape within that range. The residual shape error (deviation of DM shape from ideal first order spherical shape after closed-loop calibration) varied from ~20 nm for small-amplitude shapes to more than 80 nm for large amplitude shapes. This variation is plotted in Fig. 4.

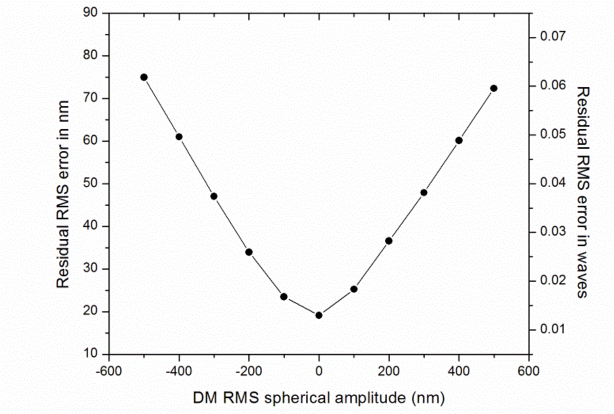

Fig. 4. Closed-loop DM calibration results. Residual shape error in nanometers and waves (assuming 1310 nm illumination) is plotted as a function of DM first order spherical shape amplitude. Errors are negligible for +/− 250 nm RMS shapes, corresponding to wavefront errors of +/−500 nm. The range of errors is simulated in Fig. 2.

3.2 Sample and aSIL microscope setup

The samples used in this study are custom-made resolution targets. They were fabricated using electron beam lithography and aluminum deposition on a Si wafer. The patterns on the chip are sets of parallel lines with pitch from 100 nm to 400 nm. Figure 5 shows a scanning electron microscope image of a subsection of the resolution target, with pitch indications to the left of the patterns. The duty cycle of the line width and line spacing is 50%. Each line is about 2.5 µm long.

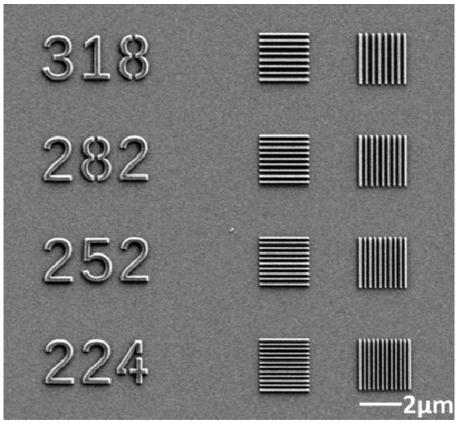

Fig. 5. SEM micrograph of the fabricated resolution test patterns with pitch of the patterned lines marked to the left.

The microscope is set up in a confocal scanning aSIL configuration, as shown in Fig. 6: 1310nm light from a fiber-coupled laser is collimated and directed to the DM. Between the DM and laser, polarization optics and beam splitters are used to direct the light appropriately. The DM is optically conjugated to the mid-position of two galvanometric scanning mirrors (Thorlabs 2D Scanning Galvo Mirror System) using a unity magnification lens pair. The mid-position of the two galvanometric scanning mirrors is conjugated to the pupil of the backing objective (0.4NA 20 × Mitutoyo Plan Apo NIR Infinity-Corrected Objective) using a 1.33 × magnification lens pair. Light focuses through the Si aSIL, nominally to the aplanatic plane. Reflected light returns along the same path so that the DM can be used to correct spherical aberrations both in the illumination path and detection path [27]. The system is controlled through LabView.

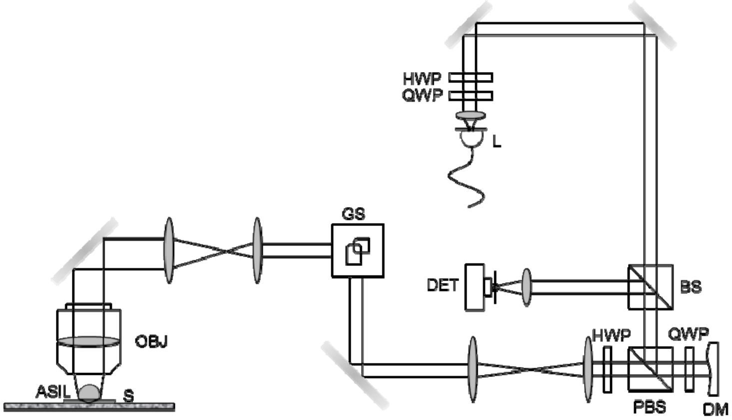

Fig. 6. Schematic of the aSIL confocal scanning microscope. ASIL: Aplanatic solid immersion lens. BS: Beam splitter. DET: Detector. DM: Deformable mirror. GS: Galvo scanning mirrors.

HWP: Half wave plate. L: Laser 1310nm. OBJ: Objective. PBS: Polarizing beam splitter. QWP: Quarter wave plate. S: Sample.

We studied the aberration effect on imaging by choosing samples that had known thickness mismatch, and we used the DM to compensate the spherical aberration introduced by the sample thickness mismatch.

4. Results

For an experimental demonstration, we chose a sample that was 11 μm thinner than the ideal thickness, and used a silicon aSIL with 1310 nm illumination. The ray tracing simulated aberrations for on-axis and off-axis aberrations are shown in Table 1, indicating that ~275 nm of first order spherical aberration will be required to compensate the effect of the sample thickness error. Without aberrations, the theoretical resolution based on the Sparrow criterion (0.61 λ/NA) for this microscope configuration is 228 nm. In our experimental result, without compensation the 318 nm resolution target group is barely resolvable due to the presence of spherical aberration. Because spherical aberration shifts the plane of best focus, one needs to translate the stage to minimize focus error in addition to applying a compensating spherical aberration correction to the DM. This was done though an iterative approach by iteratively applying different amplitudes of spherical shape to the DM and translating the sample stage to adjust focus in an effort to optimize image quality (or maximum confocal photon detector signal).

After applying a + 190 nm RMS first order spherical compensatory shape on the DM (+ 380 nm RMS wavefront correction taking the DM double path into account) and translating the stage about 100 μm away from objective, the 252 nm group can be resolved. In addition to more resolving power after correcting for spherical aberration, the average intensity of the image increases by 50%. The image contrast is significantly higher as well, as seen in Fig. 7. A finer 224 nm resolution group was not resolved.

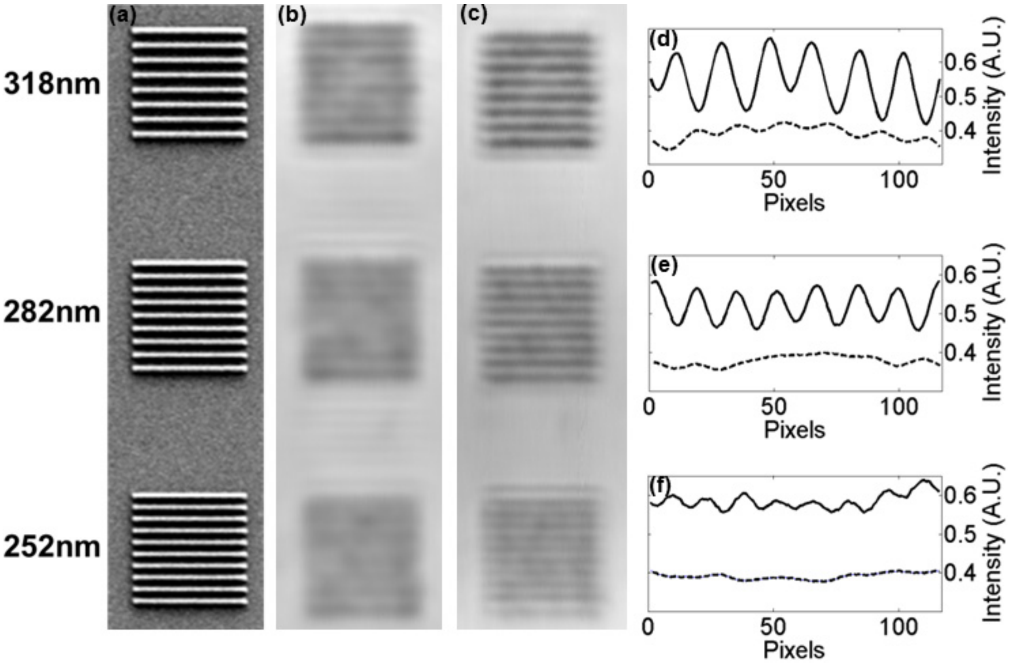

Fig. 7. Comparison before and after applying + 190 nm RMS first order spherical aberration correction. (a): SEM image showing the region of interest. (b): aSIL microscope image obtained before spherical aberration correction. (c): aSIL microscope image obtained after

spherical aberration correction. (d): Line cut comparison on group 318 nm. (e): Line cut comparison on group 282 nm. (f): Line cut comparison on group 252 nm.

Table 1. Aberration simulation of Si aSIL on −11 µm Si sample through ray tracing software (unit: wave)

Aberration	On-axis Ray	Off-axis Ray (+/−15µm FOV)
Defocus	0	0
Astigmatism	0	0.016
Coma	0	−0.088
Trefoil	0	0.001
1st Spherical	−0.210	−0.213
2nd Coma	0	−0.018
2nd Spherical	−0.024	−0.026
3rd Spherical	−0.004	−0.005

5. Discussion

In this study, we only considered first order spherical aberration compensation, which is mainly introduced by sample thickness error. There can potentially be other types of aberrations in the system which remain uncorrected, such as off-axis aberrations due to confocal scanning, higher order spherical aberrations due to sample large thickness mismatch, and indices mismatch using different material aSIL on Si sample, etc.

For example, Fig. 8 shows image comparison with and without DM spherical aberration correction using the same Si resolution target sample that was used to obtain the data shown in Fig. 7. But in this experiment, a GaAs aSIL and 1064 nm laser were used and the measured thickness mismatch is about −44 µm. The index of refraction mismatch between the GaAs aSIL and the Si sample can be expected to introduce additional aberration. Table 2 shows the Zemax simulation on this particular case. With aberration compensation, the finest resolvable group is at 252 nm (compared to a theoretical resolution of 185 nm), and worse than the image quality achieved with a Si aSIL at 1310 nm. Moreover, even after compensation the image quality degrades quickly from the center to the edge of the image, which implies that large off-axis aberrations exists in the system. This is confirmed by the off-axis simulation, which predicts several hundred nanometers of Coma variation (Zernike terms 7 and 8) for this configuration. Unfortunately, due to the specular reflection from the sample and air interface, those odd-symmetry aberrations cannot be fixed unless a second DM is used [28].

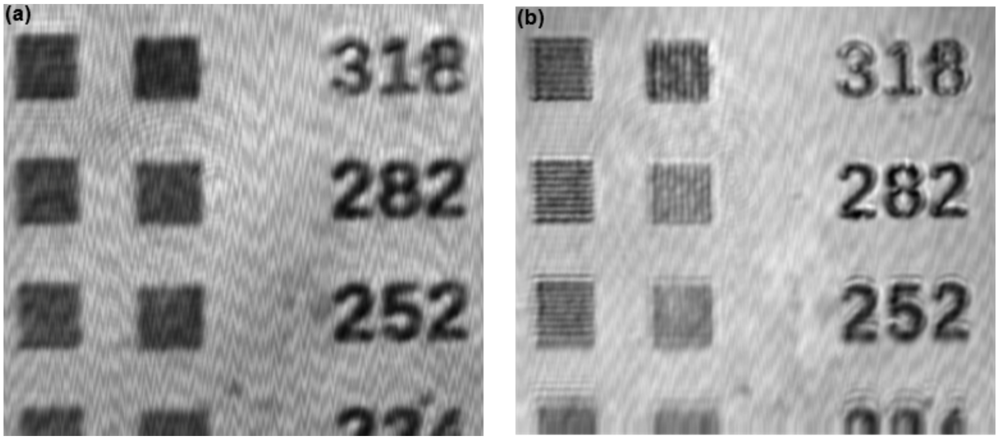

Fig. 8. Comparison on (a) before and (b) after applying a + 360 nm first order spherical aberration correction.

#197853 - $15.00 USD Received 1 Oct 2013; revised 31 Oct 2013; accepted 31 Oct 2013; published 8 Nov 2013

Table 2. Aberration simulation of GaAs aSIL on –44 µm Si sample through ray tracing software (unit: wave)

Aberration	On-axis Ray	Off-axis Ray (+/–15µm FOV)
Defocus	0	0
Astigmatism	0	0.040
Coma	0	–0.332
Trefoil	0	0.001
1st Spherical	–0.895	–0.908
2nd Coma	0	–0.031
2nd Spherical	–0.038	–0.043
3rd Spherical	–0.005	–0.007

In addition to correcting spherical aberration using open-loop DM shapes, other closed-loop adaptive optics approaches, such as image-based optimization and wavefront sensing, are also promising. Image-based optimization uses quality metric as feedback to improve image. This method requires quality metric to be generic, robust and sensitive to changes. For example, a metric that uses prior knowledge of the sample, such as layout or CAD information of the DUT, is a good candidate for this image-based optimization purpose. Because of the double pass effect from a sample specular reflection, it is possible that the wavefront sensor can only sense either the odd or even symmetry aberrations depending on the sensor's location [28]. Therefore, one should consider this limitation before implement wavefront sensing.

6. Conclusion

Spherical aberration correction has been demonstrated on an aSIL confocal scanning microscope using a MEMS deformable mirror when the substrate thickness deviates from designed thickness. We have shown nearly diffraction-limited imaging performance with higher image intensity and higher contrast after aberration compensation. Also, practical considerations for using aSIL with potentially larger and higher-order aberrations are discussed. This technique can be used for high NA solid immersion microscopy where aSIL is needed.

Acknowledgments

This work is supported by the Intelligence Advanced Research Projects Activity (IARPA) via Air Force Research Laboratory (AFRL) with contract number: FA8650-11-C-7102. We would like to thank Devin Brown from Georgia Institute of Technology for fabricating the resolution target sample. We would also like to thank Dr. Michael Grogan for developing the imaging software in LabView, and Abdulkadir Yurt for helpful discussion. Dr. Thomas Bifano acknowledges a financial interest in Boston Micromachines Corporation.